NASA SP-289

APOLLO 15

Preliminary Science Report

PREPARED BY

NASA MANNED SPACECRAFT CENTER

Scientific and Technical Information Office 1972

NATIONAL AERONAUTICS AND SPACE ADMINISTRATION

Washington, D.C.

17. X-Ray Fluorescence Experiment

I. Adler,[a†] *J. Trombka,*[a] *J. Gerard,*[ab] *R. Schmadebeck,*[a]
P. Lowman,[a] *H. Blodgett,*[a] *L. Yin,*[a] *E. Eller,*[a] *R. Lamothe,*[a]
P. Gorenstein,[c] *P. Bjorkholm,*[c] *B. Harris,*[c] *and H. Gursky*[c]

The X-ray fluorescence spectrometer, carried in the scientific instrument module (SIM) bay of the command-service module (CSM), was used principally for orbital mapping of the lunar-surface composition and, secondarily, for X-ray astronomical observations during transearth coast. The lunar-surface measurements involved observations of the intensity and characteristic energy distribution of the secondary or fluorescent X-rays produced by the interaction of solar X-rays with the lunar surface. The astronomical observations consisted of relatively long periods of X-ray measurement of preselected galactic sources such as Cygnus (Cyg X-1) and Scorpius (Sco X-1) and of the galactic poles.

COMPOSITIONAL MAPPING OF THE LUNAR SURFACE

Theoretical Basis

The production of X-rays characteristic of an element can be understood in terms of the simple Bohr theory of the atom. The electrons surround the nucleus in an orderly fashion in a series of shells – K, L, M, and so forth – from the nucleus out to the valence shell. Within any given atom, the binding energy decreases from the inner electrons, where the binding energy is greatest, to the outer shells.

Because characteristic X-ray spectra result from the filling of the vacancies produced by the ejection of these inner-shell electrons, greater input energy is required to excite the K spectrum than is required to excite the L spectrum, and even less energy is required to excite the M spectrum. The situation is summarized in figure 17-1. Tabulated within figure 17-1 are the absorption-edge energies E_k, which are required to ionize the atoms in the K shell, and $E(K_\alpha)$, the energies of the resulting X-ray lines. Therefore, to produce the characteristic X-rays, an incident energy in excess of the binding energy of the electron is necessary.

In the fluorescence experiment described in this section, the production of the characteristic X-rays follows the interaction of solar X-rays with the lunar surface. The result of numerous calculations indicates that the typical solar X-ray spectrum is energetically

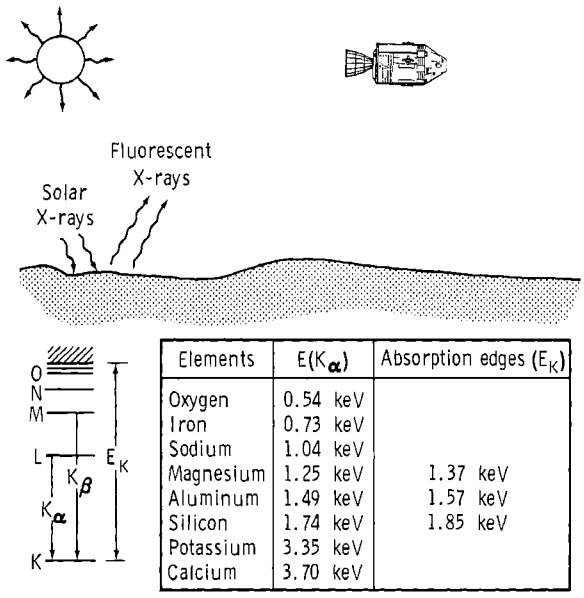

Elements	$E(K_\alpha)$	Absorption edges (E_K)
Oxygen	0.54 keV	
Iron	0.73 keV	
Sodium	1.04 keV	
Magnesium	1.25 keV	1.37 keV
Aluminum	1.49 keV	1.57 keV
Silicon	1.74 keV	1.85 keV
Potassium	3.35 keV	
Calcium	3.70 keV	

FIGURE 17-1.–The X-ray fluorescence at the lunar surface. On the left are inner electron transitions resulting in characteristic K X-ray spectra. Absorption-edge energies and the energies of the resulting X-ray lines are tabulated.

[a]NASA Goddard Space Flight Center.
[b]National Academy of Sciences.
[c]American Science and Engineering.
[†]Principal investigator.

capable of producing measurable amounts of characteristic X-rays from all the abundant elements with atomic numbers of approximately 14 (silicon (Si)) or less. During brief periods of more intense solar activity, observation of radiation from elements of higher atomic number also should be possible.

In the final analysis of the data, however, some features of the X-ray production of the Sun must be considered in greater detail. The solar X-ray flux varies greatly on time scales of minutes to hours. In addition, systematic changes occur that are associated with the 11-yr solar cycle.

This long-term trend is shown in figure 17-2 (ref. 17-1). A curve of the smoothed sunspot number is shown on the same axis as the observed X-ray intensity. A definite correlation exists between the sunspot number and the X-ray intensity, so the extrapolated smoothed sunspot number is an indication of the expected solar intensity for the next few years.

The solar X-ray flux, with low-resolution instruments such as proportional counters, decreases with increasing energy. If a strictly thermal mechanism of production is assumed, variable coronal temperatures are found somewhere between 10^6 to 10^7 K. Such variations in temperature produce changes in both flux and spectral composition. Thus, changes must be expected not only in fluorescent intensities but in the relative intensities from the various elements being observed. For example, if the solar spectrum hardens (larger fluxes of higher energies) or if there is an increase in characteristic line intensities on the high-energy side of the absorption edge of the heavier element, an enhancement of the intensities from the heavier elements relative to the lighter ones would be observed.

An X-ray monitor was used to follow the possible variation in solar X-ray intensity and spectral shape. In addition, detailed simultaneous measurements of the solar X-ray spectrum were obtained in flight during the mission from the various Explorer satellites that measure solar radiation.

An estimate of the emitted solar X-ray flux for an assumed temperature of 4×10^6 K and a gray-body emitter is shown in figure 17-3. Superimposed on this

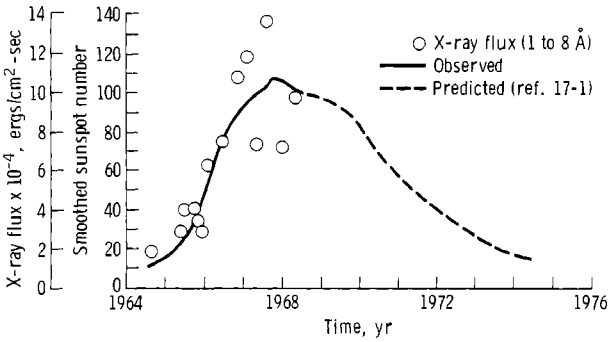

FIGURE 17-2.–Smoothed sunspot number and observed X-ray intensity as a function of time during the solar cycle.

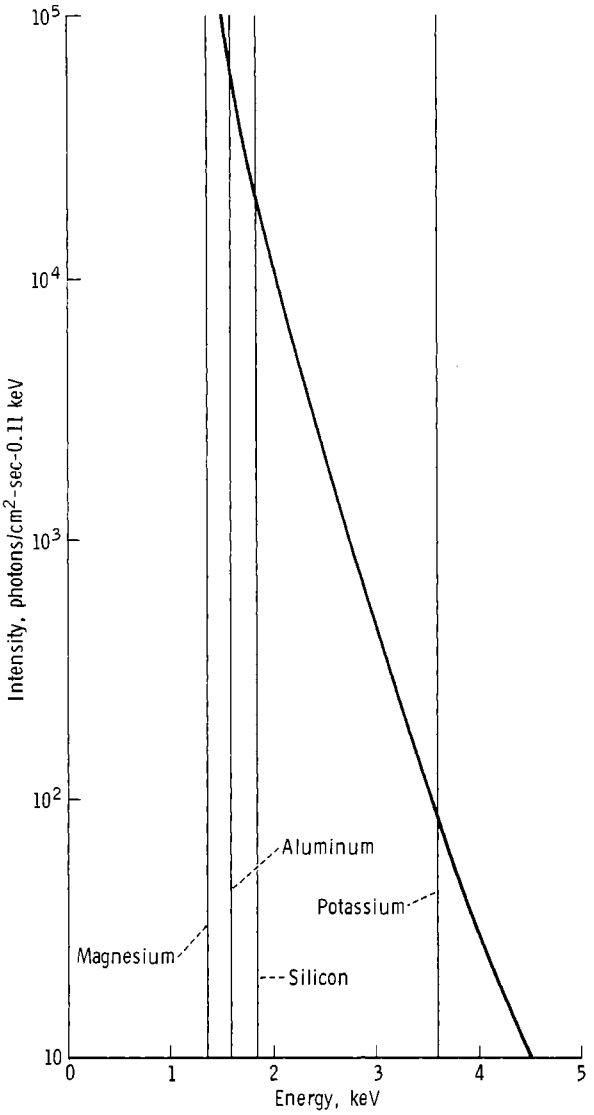

FIGURE 17-3.–The solar spectrum calculated for a coronal temperature of 4×10^6 K. Lines showing the positions of the absorption edges for Mg, Al, Si, and K are superimposed.

curve along the energy axis are the K-shell absorption edges for magnesium (Mg), aluminum (Al), Si, and potassium (K). Only the solar X-rays with energies on the high side of the absorption edges are capable of exciting these elements and to a degree depending on the incident flux and ionization cross section. Therefore, under quiet-Sun conditions, the solar flux is most suitable for exciting the light elements, including the major rock-forming elements Si, Al, and Mg.

Equipment is used to measure both X-ray intensities and energies because the Sun will produce secondary X-rays characteristic of such rock-forming elements as Mg, Al, and Si. A Bragg spectrometer cannot be used for precise wavelength selection because the amounts of secondary X-rays produced are relatively small. Instead, low-resolution but high-sensitivity techniques are required, such as proportional counters and pulse-height analysis (ref. 17-2). Selected X-ray filters are also used to provide additional energy discrimination.

Description of the Instrument

The X-ray fluorescence and alpha-particle experiment is shown in figure 17-4, and a functional configuration of the spectrometer is shown in figure 17-5. The spectrometer consists of three main subsystems.

(1) Three large-area proportional counters that have state-of-the-art energy resolution and 0.0025-cm-thick beryllium (Be) windows

(2) A set of large-area filters for energy discrimination among the characteristic X-rays of Al, Si, and Mg

(3) A data-handling system for count accumulation, sorting into eight pulse-height channels, and, finally, for relaying the data to the spacecraft telemetry

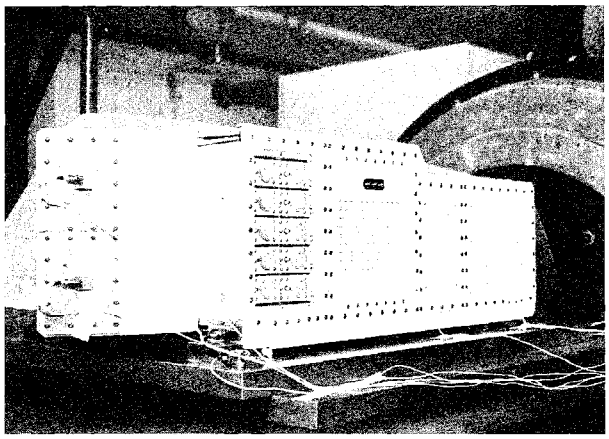

FIGURE 17-4.–The X-ray fluorescence and alpha-particle experiment. The 10 alpha-particle detectors are shown to the left of the proportional counter collimator.

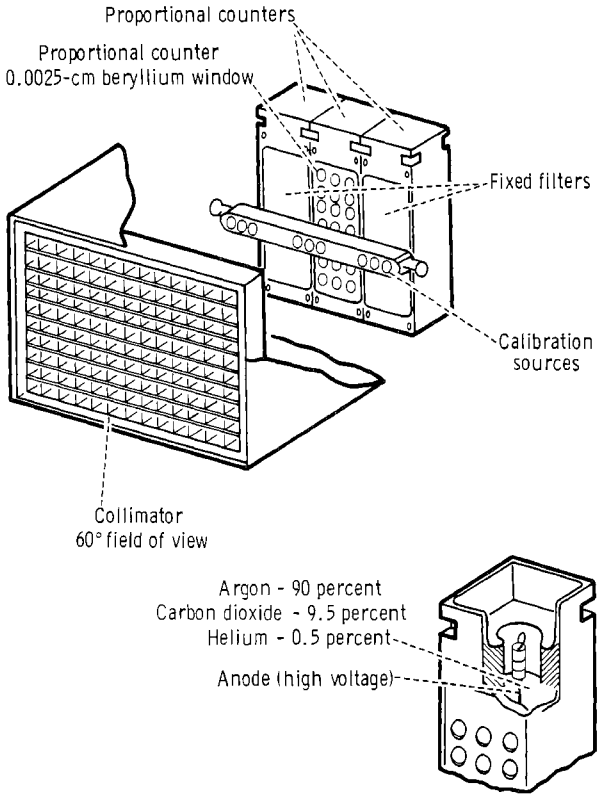

FIGURE 17-5.–Functional configuration of the X-ray spectrometer.

The X-ray detector assembly consists of three proportional-counter detectors, two X-ray filters, mechanical collimators, an inflight calibration device, temperature monitors, and associated electronics. The detector assembly senses X-rays emitted from the lunar surface and converts the X-rays to voltage pulses that are processed in the X-ray processor assembly. Provisions for inflight calibration are made by means of programed calibration sources, which, upon internal command, assume a position in front of the three detectors for calibration of gain, resolution, and efficiency. Thermistors located at strategic points sense the temperature of the detector assembly for telemetry monitoring and temperature control of the detectors by means of heaters located near the proportional counter windows.

The three proportional counters are identical, each having an effective window area of approximately 25 cm^2. The window consists of 0.0025-cm-thick Be. The proportional counters are filled to a pressure of 1 atm with the standard P-10 mixture of 90 percent argon, 9.5 percent carbon dioxide, and 0.5 percent helium. To change the wavelength response, filters are mounted across the Be window aperture on two of the proportional counters. The filters consist of a Mg foil and an Al foil 5.08×10^{-4} to 1.27×10^{-3} cm thick. The third counter does not contain a filter. A single collimator assembly is used to define the field of view (FOV) of the three proportional counters as a single unit. The collimator consists of multicellular baffles that combine a large sensitive area and high resolution but are restricted in FOV. The FOV determines the total flux recorded from the lunar surface and the spatial resolution. The FOV is specified as $\pm 30^\circ$ full width, half maximum (FWHM), in two perpendicular directions. The FWHM is the total angular width at which the collimator drops to one-half of its peak response.

The X-ray photons passing through a proportional-counter Be window ionize the gas inside by an amount proportional to the X-ray photon energy. A very stable high-voltage power supply provides a bias voltage for the operation of the proportional counters. This high voltage across the counter produces an electrical-field gradient and, hence, a multiplication effect that results in a charge output proportional to the incident X-ray energy. A charge-sensitive preamplifier that converts the input charge to an output pulse by storing it on an integrating capacitor is mounted on each proportional counter. This pulse has a fast rise time, determined primarily by the response of the preamplifier; a slow decay, determined by the integrator decay time; and an amplitude proportional to the X-ray energy. The preamplifier gain is set for an output scale factor of approximately 0.2 V/keV. Each of the preamplifier outputs is applied to the X-ray processor assembly that sorts the outputs according to the peak amplitude level.

The inflight calibration device consists of a calibration rod with radioactive sources (Mg and manganese-K radiation) that normally face away from the proportional counters. Upon internal command from the X-ray processor assembly, the rod is rotated 180° by a solenoid driver, thereby positioning the sources to face the proportional counters. Magnetically sensitive reed relays provide feedback signals indicating when the rod is fully in the calibration mode or fully in the noncalibration mode. These feedback signals are flag bits in the data telemetry output. The calibration command signal is generated in the X-ray processor assembly. The calibration cycle repeats every 16 min and continues 64 sec.

The X-ray processor assembly processes X-ray data received from the detector assembly and from the solar monitor. The lunar X-ray data and the solar X-ray data from the solar monitor are sorted, counted, stored, and sent to telemetry. Processing of the data from one detector is shown in a functional block diagram in figure 17-6. The pulse received from the charge-sensitive preamplifier is amplified and operates as many as eight voltage discriminators, depending on the voltage level. The discriminator outputs are processed logically in the pulse-routing logic to obtain an output pulse in one of eight data channels, depending on the highest-level discriminator operated. Thus, eight channels of differential pulse-height spectra are obtained. The first seven channels are equal in width, and the eighth channel contains the integral number of events with energies greater than channel 7. The pulses from each data channel are counted by the counters in the counter-shift-register logic. Every 8 sec, the contents of the counters are transferred to the shift registers, and the counters are reset. The data are then sequentially shifted out of the shift registers to telemetry at a 10-word/sec rate. Each telemetry word consists of eight bits. Each counter is 16 bits long, thereby supplying two telemetry words. The telemetry-word-output sequence is divided into four groups of 20 words each. The groups are obtained from the 20-word-long shift registers that are sequentially gated through the output multiplexer by the main timing. Each pulse from the charge-sensitive preamplifier is also processed by a pulse-shape discriminator (PSD) that distinguishes X-ray events from background. The PSD gates off the pulse-routing logic, thus preventing non X-ray events from being counted.

Data transmitted from the CSM are recorded at ground stations on magnetic tape. As raw spectral data and ground navigational data are obtained, ephemeris data are derived. The X-rays observed by each of the three lunar detectors are sorted into seven equal-interval energy channels. The bare detector is

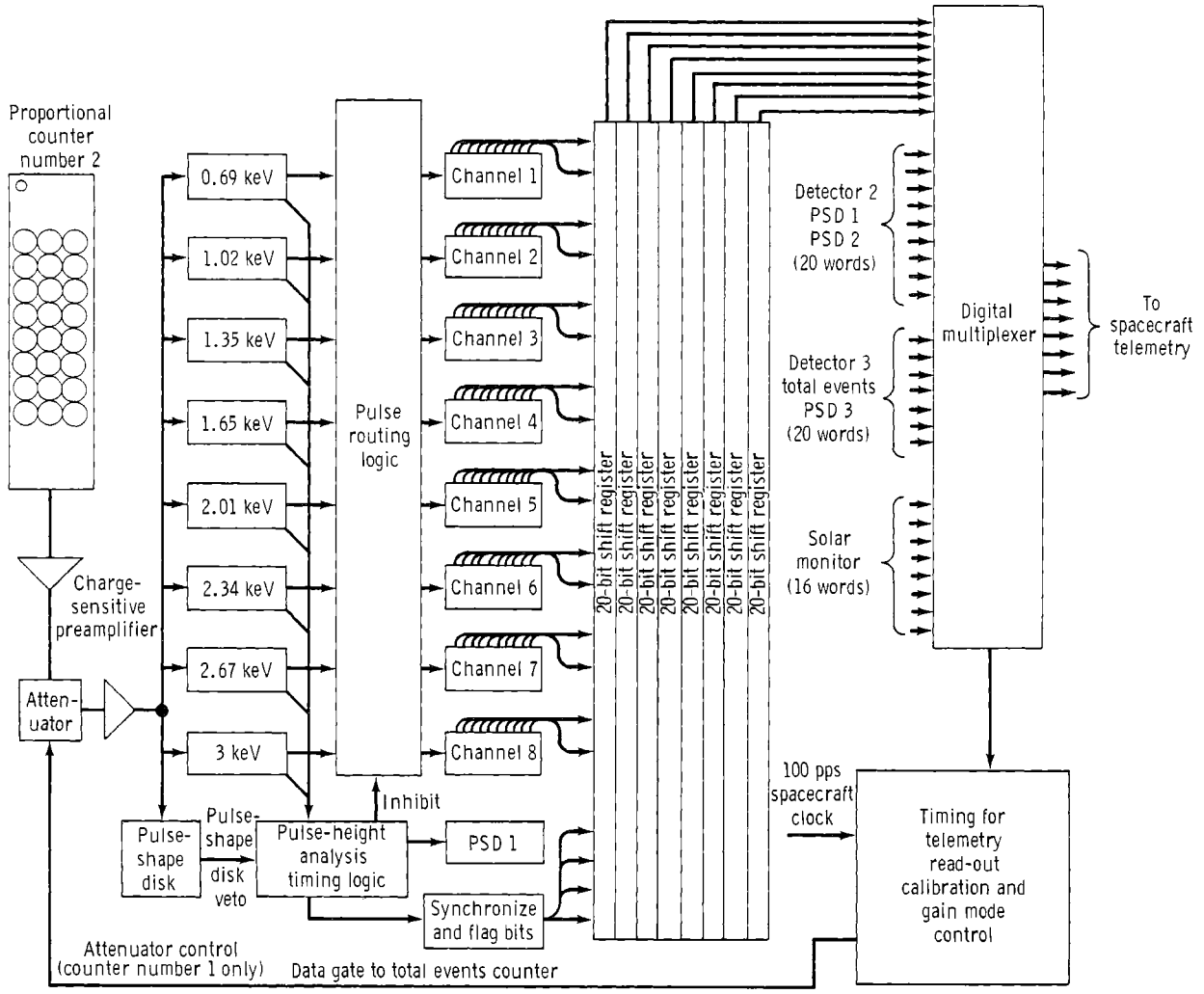

FIGURE 17-6.–Block diagram showing the data flow in the X-ray spectrometer.

operated in two modes: the high-gain (normal) mode and the attenuate mode. After the initial turnon, the bare detector operates 9.87 sec in the attenuate mode, covering a range of approximately 1.5 to 5.5 keV. At the end of this cycle, the bare detector automatically goes into the normal mode, which covers the range 0.75 to 2.75 keV. During flight, the bare detector automatically operates for 6 hr in the normal mode and 2 hr in the attenuate mode. The filtered surface detectors continuously cover the spectral range of 0.75 to 2.75 keV. The solar monitor also covers a range of approximately 1 to 3 keV.

The printout indicates the number of pulses of a given energy that were observed for each detector in a given energy channel for a given measurement interval. Histograms that are subsequently reduced by alternate techniques to line intensities and finally to chemical concentrations can be plotted from this printout.

Operation of the Experiment

The X-ray experiment began to function 84 hr into the flight, during the third revolution around the Moon. From 84 to 102 hr ground elapsed time (GET), the orbit was approximately 8 by 60 n. mi. After 102 hr, the orbit was circularized and maintained at approximately 60 n. mi. until transearth coast. During the orbital period, more than 100 hr of surface measurements were made. The solar-monitor detector was used for simultaneous monitoring of

solar X-ray flux. Lunar-far-side data were recorded on magnetic tape and telemetered on the near side. Because both record and playback occurred in the same tape direction, the tape recorder was rewound each time, causing some loss of far-side data. To maximize the amount of ground coverage, an attempt was made to alternate the rewind operation so that the operation would occur either after signal loss or before signal acquisition. Data loss in the X-ray experiment occurred only when the tape recorder was rewound on the illuminated portion of the far side; however, the data loss has not seriously compromised the experiment.

The data from the experiment were displayed almost real time as a numeric display on a cathode-ray-tube monitor. The data were displayed in the form of running sums for the seven energy channels for each of the four detectors. The data, supplied as hard-copy printout, were updated at 1-min intervals and at regular intervals of approximately 4 hr. This preliminary report is based on the reduction of this quick-look data. The results presented in this report are, of necessity, degraded in terms of spatial resolution along the projected ground track because each minute represents a 3° longitudinal displacement. The processing of prime data, obtained at 8-sec intervals, should yield improved spatial information.

Results

Alternate procedures for processing the flight information are available, depending on the degree of sophistication warranted by the data. The data in this report have been treated in a very simple fashion based on the energy discrimination afforded by the selected X-ray filters. The following assumptions have been made.

(1) All three proportional counters have identical characteristics

(2) The detectors are 100-percent efficient for the radiation transmitted through the detector window

(3) Background corrections can be made using the measured far-side fluxes

(4) The effect of X-ray scattering on the Al/Si intensity ratios, although authentic, can be ignored in these first estimates

Based on these assumptions, three simultaneous expressions of the following form were written.

$$I_{Bare} = T_{Al}^{Be} I_{Al} + T_{Mg}^{Be} I_{Mg} + T_{Si}^{Be} I_{Si} \qquad (17\text{-}1)$$

$$I_{Al\ filter} = T_{Al}^{Be}\left(I_{Al} T_{Al}^{Al}\right) + T_{Mg}^{Be}\left(I_{Mg} T_{Mg}^{Al}\right) + T_{Si}^{Be}\left(I_{Si} T_{Si}^{Al}\right) \qquad (17\text{-}2)$$

$$I_{Mg\ filter} = T_{Al}^{Be}\left(I_{Al} T_{Al}^{Mg}\right) + T_{Mg}^{Be}\left(I_{Mg} T_{Mg}^{Mg}\right) + T_{Si}^{Be}\left(I_{Si} T_{Si}^{Mg}\right) \qquad (17\text{-}3)$$

I_{Bare}, $I_{Al\ filter}$, and $I_{Mg\ filter}$ are, respectively, the total intensities summed over all seven channels for the bare detector, the detector with the Al filter, and the detector with the Mg filter.

T_{Al}^{Be}, T_{Mg}^{Be} and T_{Si}^{Be} are, respectively, the transmission factors of the detector Be windows to the characteristics Al, Mg, and Si radiation.

T_{Al}^{Al}, T_{Mg}^{Al}, and so forth are, respectively, the transmission factors of the Al filter for the characteristic Al, Mg, and so forth radiation.

T_{Al}^{Mg}, T_{Mg}^{Mg}, and so forth are, respectively, the transmission factors of the Mg filter for the characteristic Al, Mg, and so forth radiation.

A least-squares analysis method was used to solve the previous equations because an estimation of the statistical validity of the results is easily obtained. In solving the equations, a number of Al/Si and Mg/Si intensity ratios were obtained. These are X-ray intensity ratios, not elemental ratios, that are proportional to each other but are not equal.

As suggested in the experiment description, the flux intensity and energy distribution of the solar X-rays were expected to have a significant effect on the nature of the fluorescent X-rays. The purpose of the solar monitor was to observe the intensity and energy distribution of the solar X-rays as a function of time, simultaneously with the surface measurements. Figure 17-7 is a plot of the integrated intensities registered by the solar monitor for the period corresponding to the surface measurements. These values were observed at the subsolar point. A plot is also shown for comparing the surface intensities as observed with the solar detector. With the exception of revolutions 67 and 73, the solar flux was fairly stable, varying less than ±30 percent of the mean value. This stability was equally reflected in the surface data, which indicate a stable incident flux as well as a stable spectral distribution.

During revolutions 67 and 73, a marked increase in flux and, apparently, a hardening of the energy

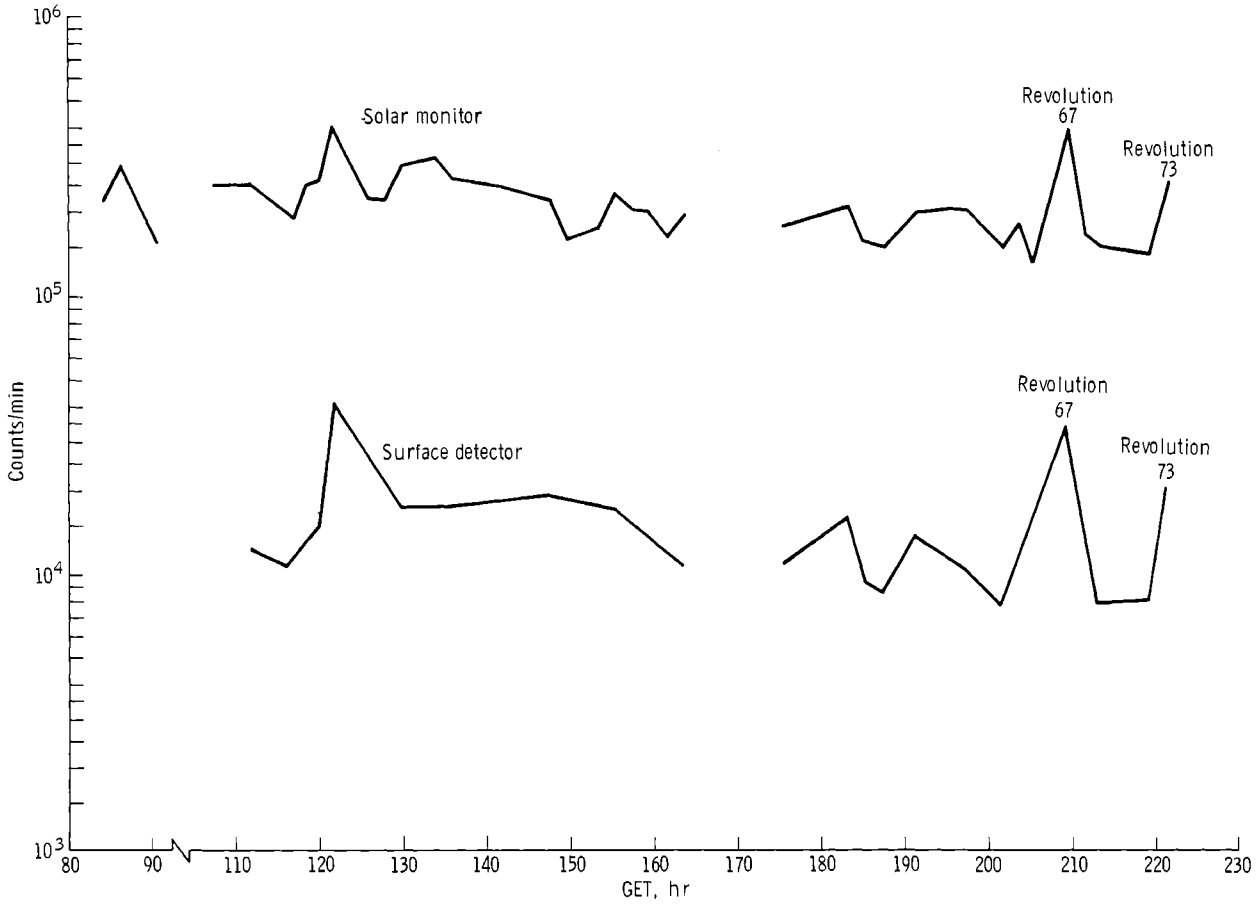

FIGURE 17-7.–Comparison of solar X-ray flux and surface flux.

spectrum occurred. This phenomenon was reflected in reduced Al/Si intensity ratios, which were probably caused by enhanced Si excitation. On subsequent revolutions, the solar-flux intensity and the Al/Si intensity ratios returned to more nearly normal values.

Some of the Al/Si intensity ratios were averaged for corresponding revolutions because of their close overlap. The agreement between values on the close ground tracks was approximately ±10 percent on the average. (The scatter is based on a 1-σ variation calculated by taking repetitive values for a given area.) An examination of the ground tracks from east to west indicates that the spacecraft passed over such features as the craters Gagarin and Tsiolkovsky; the far-side and eastern-limb highlands; the mare areas Mare Smythii, Mare Crisium, Mare Fecunditatis, Mare Tranquillitatis, Mare Serenitatis, Mare Imbrium, and Oceanus Procellarum; the Haemus Mountains; and the Apennine Mountains. The Al/Si intensity ratios varied by more than a factor of 2 between the eastern-limb highlands and the mare areas, where the ratios were the lowest.

These values are detailed in table 17-I and are plotted synoptically in figures 17-8 and 17-9. Figure 17-8 represents a northerly trajectory (revolutions 16, 26 to 28, and 34), and figure 17-9 represents a more southerly course (revolutions 63, 64, and 72). The following observations can be made.

(1) The Al/Si intensity ratios are lowest over the mare areas and highest over the nonmare areas (an average of 0.67 as opposed to 1.13). The extremes vary from 0.58 to 1.37, by a factor of more than 2.3.

(2) The value for the Apennine Mountain region is 0.88, and the lower average value of the Haemus Mountains is 0.83. On the other side of the Apennine Mountains in the Archimedes Rille area, the observed value is 0.64. On either side of the Apennine

TABLE 17-I.–*Averaged Al/Si Intensity Ratios for Various Lunar Features*

Location	*Intensity ratios*
Mare areas	
Serenitatis	0.58 ± 0.06 (rim, 0.71 ± 0.05)
Imbrium	.59 ± .04
Crisium	.71 ± .02 (rim, .80 ± .09)
Tranquillitatis	.71 ± .05 (rim, .84 ± .04)
Fecunditatis	.73 ± .07 (rim, .94 ± .14)
Smythii	.73 ± .07 (rim, 1.00 ± .11)
Archimedes Rille area	.64 ± .03
Apennine Mountains	.88 ± .03
Haemus Mountains	.83 ± .10
Highlands east of Mare Serenitatis to 40° E	.80 ± .08
Highlands west and southwest of Mare Crisium	1.08 ± .13
Highlands between Mare Crisium and Mare Smythii	1.07 ± .11
Highlands between Mare Smythii and Tsiolkovsky	1.16 ± .11
Highlands east of Mare Fecunditatis	1.29 ± .23
Highlands east of Tsiolkovsky	1.37 ± .25
Area north of Schröter's Valley	.73 ± .05
Area northeast of Schröter's Valley	.64 ± .09

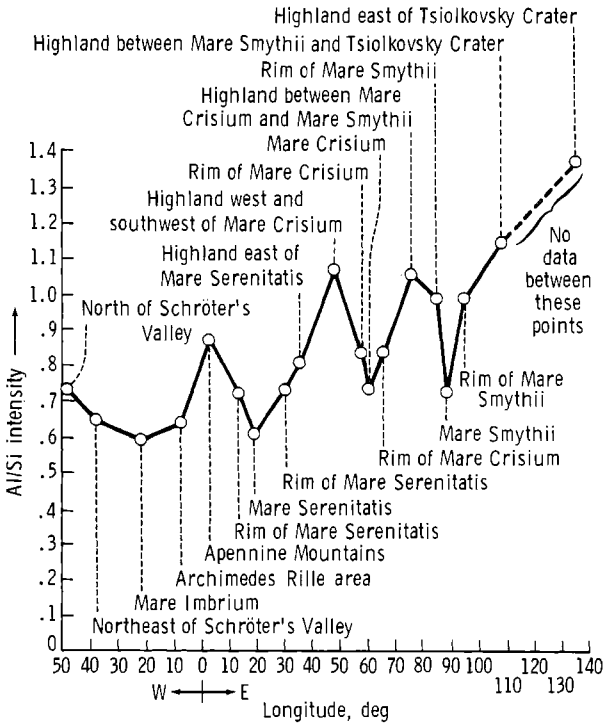

FIGURE 17-8.–Plot of Al/Si intensity ratios along a northerly ground track.

Mountains, the values for Mare Imbrium and Mare Serenitatis are 0.59 and 0.58. The Apennine Mountains have values between those of the maria and the eastern-limb highlands.

(3) An examination of the Al/Si coordinate plot reveals that the values tended to increase from the western mare areas to the eastern-limb highlands.

(4) As predicted, the rim areas are intermediately between the mare areas and the surrounding highlands.

Another interesting correlation between Al/Si ratios and albedo values along selected ground tracks is shown in figures 17-10 (ref. 17-3) and 17-11. Generally, higher Al/Si ratios correspond to higher albedo values. There are occasional deviations from these relationships caused by surface features; for example, the Copernican-type crater identified in the plot in figures 17-10 and 17-11. The composition of areas with different albedos can be inferred by using the X-ray data. It is possible, for example, to state whether the albedo variations are related to chemical differences or to the nature and, perhaps, age of a given feature.

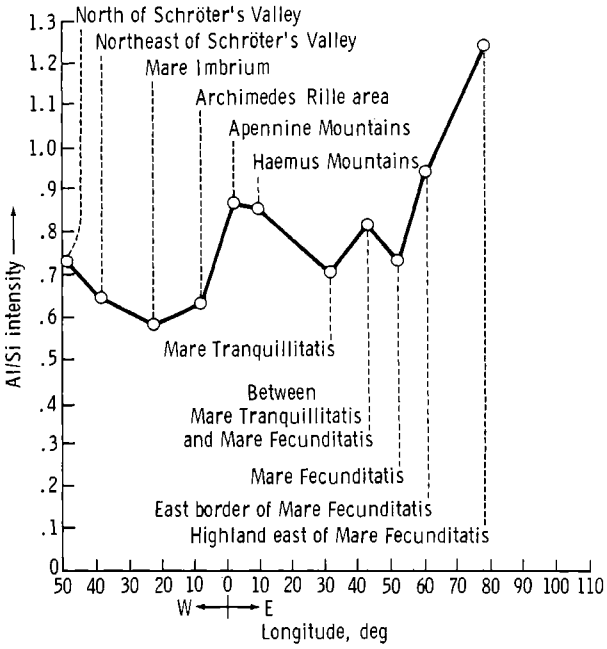

FIGURE 17-9.–Plot of Al/Si intensity ratios along a southerly ground track.

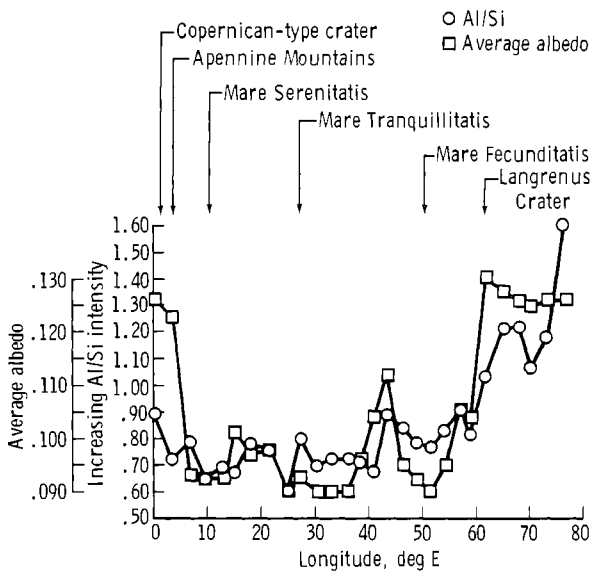

FIGURE 17-10.–Plot of Al/Si intensity ratios as a function of normal albedo values. Albedo values are for points corresponding to average Al/Si intensities for read-out intervals shown on map, for revolutions 63 and 64 (figs. 17-13 and 17-14).

Other interesting correlations exist, but the comments on these are necessarily of a very preliminary nature. An attempt has been made to plot Al/Si intensity ratios along a gravitational profile. The observed correlation indicates that the Al/Si intensity ratios vary inversely with the gravitational values. For example, the lowest Al/Si intensity ratios are found in the regions of greatest positive gravitational anomalies.

Finally, an attempt has been made to arrive at actual concentration ratios for Al/Si. These concentrations are determined by an approach that is both theoretical and empirical. The theoretical calculations are based on the assumption of a quiet Sun and a coronal temperature of 4×10^6 K. These conditions give an X-ray energy distribution, consisting of both a continuum and characteristic lines, that is consistent with the solar-monitor observations shown normalized in figure 17-12. The X-ray energy distribution and various soil compositions, as determined from the analysis of lunar samples, have been used to calculate a relationship between Al/Si intensity ratios as a function of chemical ratios.

The empirical approach involves the assumption that the soil values from the Apollo 11 site at Tranquillity Base and the Luna 16 soil values from Mare Fecunditatis are ground-truth values. With these values and the theoretically calculated slopes, the

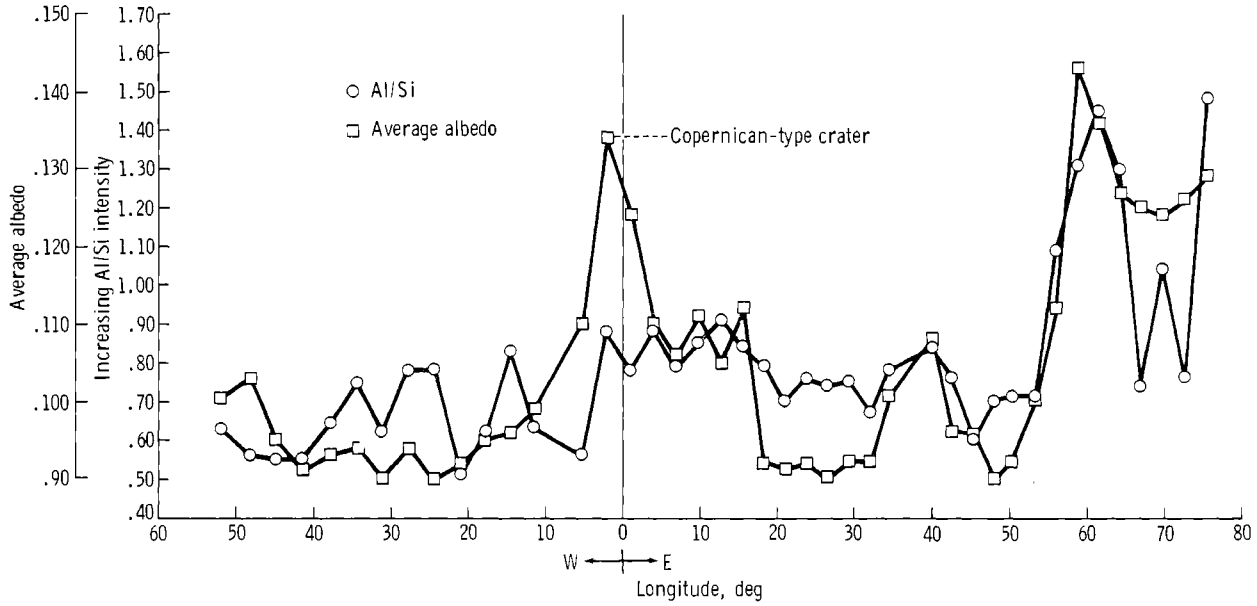

FIGURE 17-11.–Comparison of albedos and Al/Si intensity ratios for revolution 72.

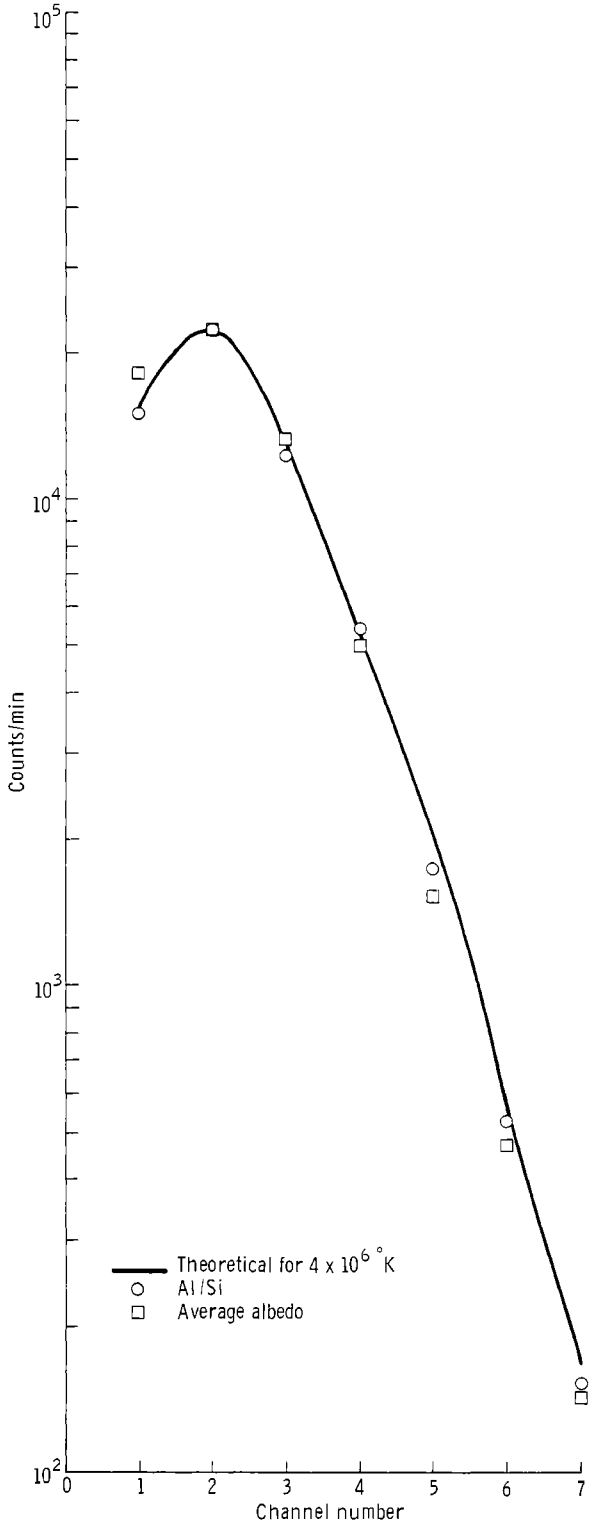

FIGURE 17-12.–Comparison of theoretical spectral distribution of detector (radiation 36° from normal) with solar monitor data taken ±12 min from subsolar point.

values of Al/Si concentrations shown in table 17-II have been determined for various parts of the Moon along the ground track. Some typical values for various lunar rocks, as determined by the chemical analysis of lunar materials, are included in this table.

The results of the X-ray fluorescence experiment are still in the preliminary stages of analysis. Never-

TABLE 17-II.–*Averaged Al/Si Concentration Ratios Calculated From the Intensity Ratios of Table 17-I*

Location	*Concentration ratios*
Mare areas	
Serenitatis	0.29 ± 0.02
Imbrium	.30 ± .03
Crisium	.37 ± .01
Tranquillitatis	.36 ± .02
Fecunditatis	.38 ± .03
Smythii	.37 ± .04
Archimedes Rille area (to Palus Putredinis)	.33 ± .01
Apennine Mountains	.46 ± .01
Haemus Mountains	.43 ± .05
Highlands east of Mare Serenitatis to 40° east	.42 ± .04
Highlands west and southeast of Mare Crisium	.56 ± .05
Highlands between Mare Crisium and Mare Smythii	.56 ± .06
Highlands between Mare Smythii and Tsiolkovsky	.60 ± .07
Highlands east of Mare Fecunditatis	.66 ± .11
Highlands east of Tsiolkovsky	.69 ± .12
Area north of Schröter's Valley	.37 ± .03
Area northeast of Schröter's Valley	.32 ± .04
Apollo 11, Mare Tranquillitatis bulk soil (ref. 17-8)	.37
Surveyor, Mare Tranquillitatis regolith (ref. 17-9)	.35
Apollo 12, Oceanus Procellarum average of soils (ref. 17-10)	.325
Luna 16, Mare Fecunditatis bulk soil (ref. 17-11)	.416
Surveyor VI, Sinus Medii regolith (ref. 17-9)	.338
Surveyor VII, rim-of-Tycho regolith (ref. 17-9)	.546
Apollo 14, Fra Mauro soils (ref. 17-12)	.413
Apollo 15, Hadley Rille-Apennine Mountains, soils (3 preliminary)	.379
Apollo 11 and 12, anorthositic gabbros	.637
Gabbroic anorthosites	.819
Anorthositic fragments	.885
Apollo 12, noritic material (ref. 17-7)	.416
Apollo12, KREEP (refs. 17-13 and 17-14)	.394
Apollo 12, dark 12013 (refs. 17-13 and 17-14)	.327

theless, some tentative interpretations are possible, especially when the data are viewed in the context of previous Apollo missions. These interpretations are based on comparisons of the relative Al/Si intensity ratios with albedo, regional geology, and analyses of returned samples; however, interpretation is subject to several limitations at this stage of analysis. Firstly, the Al/Si intensity ratios refer to large areas because the plotted data were read out at 1-min intervals and because of the 60° FOV of the X-ray spectrometer. Secondly, the X-ray fluorescence experiment is inherently a measurement of surface composition and provides no information on the subsurface composition below depths of approximately 0.1 mm except for the mixing effect of gardening.

Subject to these limitations, the following general conclusions have been formulated from the X-ray experiment about the geology and evolution of the Moon.

(1) The Al/Si ratios shown in tables 17-I and 17-II confirm that the highlands and maria do indeed have different chemical and mineralogical compositions. This conclusion is stated explicitly because, to date, there have been only two sample-return missions to the highlands (Apollo 14 and 15). Furthermore, this conclusion confirms that the albedo difference between the highlands and maria (figs. 17-13 and 17-14) is, at least in part, the expression of chemical differences. With the evidence from returned samples, the X-ray experiment indicates that two major types of materials are exposed. The high Al/Si ratios of the highlands indicate that the highlands are related to the plagioclase-rich fractions of the returned samples, whereas the low Al content of the maria is consistent with the compositional analysis of numerous mare basalts (table 17-II).

The distinct chemical and mineralogical compositional differences between the maria and the highlands limit the effectiveness of horizontal transport of material. If such a mechanism were effective for long-distance transport, the spectrometer would probably not detect compositional differences in the highlands

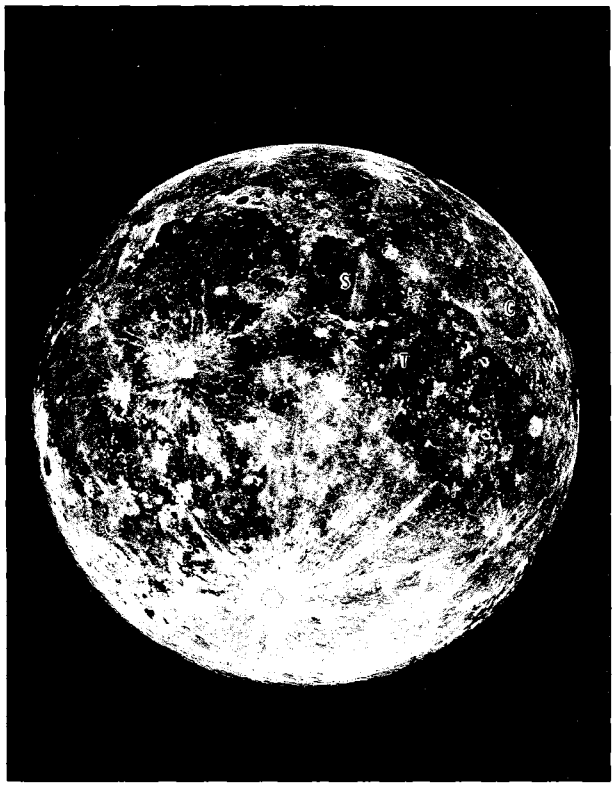

FIGURE 17-13.–Full-Moon telescopic photograph emphasizing albedo differences of the near side. Labeled areas are Mare Serenitatis (S), Mare Crisium (C), and Mare Tranquillitatis (T).

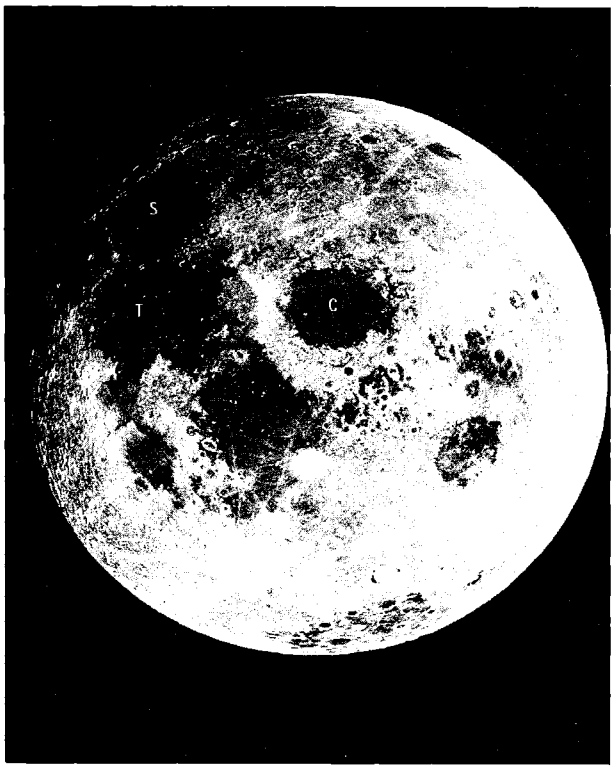

FIGURE 17-14.–High-Sun-angle photograph of east limb and part of far side, emphasizing albedo differences. Labeled areas are Mare Serenitatis (S), Mare Crisium (C), and Mare Tranquillitatis (T) (AS11-44-6667).

and maria because the instrument detects only the fine-grained surface material that would be widely distributed by electrostatic suspension. Some blurring of the mare-highland contacts probably has been caused by the cumulative effect of minor impacts. Horizontal transport, by this mechanism (minor impacts), has not carried material farther than approximately one-tenth the diameter of, for example, Mare Serenitatis.

(2) As shown in table 17-II, some indication exists of chemical differences among maria; the raw data indicate that the circular maria have less Al than the irregular maria. If these differences are authentic, they may provide information about the origin of the mare basins; the circular maria are characterized by mascons and apparent ejecta blankets whereas the irregular maria are not. The X-ray spectrometer data require more refinement for this conclusion to be confirmed; however, these data agree with the recent work of Soderblom (ref. 17-4), who found that the circular maria (red) could be distinguished spectrally from the irregular maria (blue).

(3) There appear to be systematic chemical variations within individual maria, particularly in Mare Crisium and Mare Serenitatis. The raw data indicate that the edges of these maria have a greater Al content than the centers. The possibility that these variations may be real is supported by the systematic albedo patterns in Mare Serenitatis (ref. 17-5) and more indirectly by the work of Soderblom (ref. 17-4). However, two factors require clarification. The first is the FOV, because intensity readings near mare rims may include the highland areas. The second is that the mare regolith near the borders may contain substantial amounts of ejecta from the nearby highlands. Study of X-ray data taken at 8-sec intervals may clarify this result.

(4) The Mare Imbrium ejecta blanket (Fra Mauro and Alps formations) (ref. 17-6), and possibly others, may be chemically different from the highlands outside such ejecta blankets. The intensity ratios suggest that the Al content of the blankets is intermediate between the maria and the nonejecta highlands. Assuming this difference is real, the mare-basin ejecta blankets represent more basic material derived from some depth in the Moon. However, the ejecta-blanket areas covered by the X-ray spectrometer, particularly the Haemus Mountains south of Mare Serenitatis, included substantial areas of highland-mare material (shown as Eratosthenian mare by Wilhelms, ref. 17-6). Therefore, definite conclusions concerning the composition of the mare ejecta cannot be formulated at this time.

(5) The X-ray experiment supports the belief that the first major geochemical event of the geological evolution of the Moon after its formation was the development of a global, differentiated, Al-rich crust. Despite the preliminary nature of these data, the highland areas can be pinpointed that have Al/Si ratios corresponding to analyzed lunar materials of anorthositic affinity (ref. 17-7). As shown in table 17-II (refs. 17-7 to 17-14), the anorthositic gabbros have an Al/Si ratio of 0.64; gabbroic anorthosites, 0.82; and anorthositic fragments, 0.89. Based on the X-ray fluorescence concentration ratios shown in table 17-II, the anorthositic material could be derived from any of several distinct highland areas on or near the east limb of the Moon. This assumption does not exclude other highland surfaces as the actual source of these materials but emphasizes the possibility that large definite areas exist from which they could be derived.

Negative evidence from the Apollo 15 gamma-ray experiment and the data from Luna 10 (ref. 17-15) indicate that the highlands do not have large amounts of granitic material that would otherwise be a possible explanation for the higher Al content of the highlands. Also, the scarcity of granitic compositions in samples returned to date from the Apollo 11, 12, and 14 missions and from Luna 16 is negative evidence.

Summary

Preliminary analysis of only part of the X-ray fluorescence experiment data, that pertaining to the relative Al/Si ratios, shows that the experiment has been highly successful. Major compositional differences between the maria and the highlands have been confirmed, and there are suggestions of compositional variations within both the maria and the highlands. The compositions inferred from the X-ray and gamma-ray data are consistent with the study of returned lunar samples. The main preliminary results of the X-ray fluorescence experiment are a tentative confirmation that the Moon has a differentiated highland crust of feldspathic composition, probably similar to the various materials of anorthositic affinity found in samples extracted during the Apollo 11, 12, 14, and 15 missions.

ASTRONOMICAL X-RAY OBSERVATIONS

The objective of the galactic X-ray observations is to study in detail the temporal behavior of pulsating X-ray sources. Approximately 100 sources of X-ray emission have been discovered beyond the solar system. These sources include a large variety of unusual objects, such as supernova remnants, energetic external galaxies, quasars, and a large number of sources in our galaxy that cannot be associated with any previously known class of objects. Several of these sources are detectable as emitters of radio waves or can be seen as faint stars, but emission from these sources occurs predominantly at X-ray frequencies. One of the prime objectives of astrophysics is to understand the nature of these X-ray sources. The first X-ray astronomy satellite launched by NASA, Explorer 42 (UHURU), has recently discovered rapid variability or pulsations in the output from several sources (refs. 17-16 and 17-17). The rapid variability occurs on a time scale of minutes, seconds, or less, implying that the emitting regions are very small, much smaller than the Sun, although the regions are emitting approximately a thousand times more power. Because this is such an unusual phenomenon, the rapid variability may provide the clue that is needed to understand the mechanisms that drive these sources. The objective of the Apollo observation is continuously to record the emission from several objects for a period of approximately 1 hr. The Apollo Program capability for observing time variations is unique, because the spacecraft can be pointed at the source for the entire time, whereas, UHURU can observe for only approximately 1 or 2 min per sighting. Consequently, the Apollo Program provides the capability of determining whether periodicities exist in the range of 10^1 to 10^3 sec.

Two powerful X-ray sources observed by Apollo 15, Sco X-1 and Cyg X-1, can also be seen on the Earth in other regions of the electromagnetic spectrum. Sco X-1 is detectable in both visible light and radio emission, but Cyg X-1 is detectable only in radio emission. It is known that the visible light and radio emissions are also variable, but how the light or radio variability correlates with the X-ray variability is still unknown. Specific predictions concerning the ranging of X-ray and other variability from no correlation to complete correlation are made on the basis of data obtained from special models of these X-ray objects. Consequently, to broaden the scope of the investigation, arrangements were made for ground-based observatories to monitor visible light and radio emissions simultaneously with Apollo 15 observations. The Apollo observations were made during Houston daylight hours, which is an unfavorable situation for observatories in North America. Fortunately, observatories located at more easterly points in nighttime hours were able to acquire Sco X-1 and Cyg X-1 data simultaneously with Apollo 15 observations. The optical flux from Sco X-1 was observed by the Crimean Astrophysical Observatory in the U.S.S.R. and by the Wise Observatory in Israel with time resolutions of 20 sec and 4 min, respectively. Radio emissions from Sco X-1 and Cyg X-1 were observed by the Westerbork Observatory in the Netherlands. The specific objective of the first phase of the analysis is to apply Fourier analysis to all these data.

Theoretical Basis

The observation of rapid variations in several galactic X-ray sources is rather conclusive evidence that the sources are highly compact objects. Significant intensity variations within a few seconds or less indicate that the diameter of the X-ray emitting region is comparable to the emitting region of the Earth or smaller, although energy is being emitted at a rate of a thousand Suns. Because the behavior of the pulsating X-ray sources is rather phenomenal and not easily explained, the simplest approach to a valid explanation is to attempt an association of these sources with strange, previously known objects. The small size of these sources indicates that the X-ray source is possibly a white dwarf, a neutron star, or the hypothetical black hole. However, associating the pulsating X-ray source with any of these three objects or explaining the profuse radiation of energy presents rather formidable problems. The most common of the three sources are the white dwarfs; however, no white dwarf has been observed to radiate energy so copiously, to emit X-rays, or to vary so rapidly. If the pulsating X-ray sources are white dwarfs, the sources represent a rather unique subgroup. No nebulosity surrounds the X-ray source (which would suggest that a supernova explosion has taken place), so the source cannot be explained as a neutron star (the superdense core remnant of a supernova explosion). The X-ray source is possibly an old neutron-star remnant in which the surrounding nebulosity has dissipated. However, the older, known neutron stars do not emit

X-rays, and their radio emissions show a rather stable, well-defined period. Black holes are the hypothetical, infinitely dense remnants of supernova explosions of massive stars. Although the intense gravitational field of a black hole does not allow radiation to be emitted, the suggestion has been made that the accretion of matter from a nearby neighbor onto the black hole would result in an irregularly varying X-ray source. In fact, according to some viewpoints, this process of accretion is the only way in which a black hole can be detected.

One important objective is to determine the mechanism that causes such a small object to radiate energy so copiously. The X-rays presumably come from either the thermalization of high-velocity matter accreting onto a small object or from the dissipation of rotational or vibrational mechanical energy contained in the object itself. Possibly, a study of the time variability will answer this question. Each mechanism would predict a frequency spectrum. An explanation based on the dissipation of rotational energy may result in a rather regular variability, whereas vibrational energy or matter accretion as the source would indicate a different kind of time variability. The time variability can be studied as a function of X-ray energy. The X-ray detectors are sensitive to the range 1 to 3 keV. The presence of filters over two of the three detectors permits the effective subdivision of this range into three parts for the analysis.

The bright X-ray source, Sco X-1, is an especially interesting candidate for the Apollo studies because this source is detectable as a 12th-magnitude blue star in visible light, is observable in infrared radiation, and is a radio source. Thus, the observational power of a broad range of astronomical disciplines can be used to study this object. An understanding of the mechanisms driving Sco X-1 may provide a basis for understanding many galactic sources. No rapid variability has been detected from Sco X-1. However, in the Apollo Program, it is possible to observe Sco X-1 in a new time regime and to look for variability on the order of a few minutes.

Equipment

The same instrumentation is used in the Apollo astronomical X-ray observations as in the X-ray fluorescence studies of lunar-surface chemical composition. A detailed description of the instrument has been given in the first part of this section.

Description of the Instrument

The FOV of the detectors is limited to an angular acceptance of 30° by 30° (FWHM) by mechanical slat collimators. Energy from a cosmic source reaches the counters as a perfectly parallel beam and is seen at maximum intensity when the direction is normal to the plane of the counters. The intensity is reduced off axis by the cosine and shadowing effects of the collimators. When the angle of the source exceeds 60° off axis, no counts are detected; however, variation of the angle will cause an apparent variation in the intensity of an otherwise steady source.

The nature of the X-ray emission from two of the Apollo 15 targets, Sco X-1 and Cyg X-1, and from most cosmic X-ray sources is such that the unfiltered detector counts more strongly than the two that are filtered. Most of the useful data on cosmic sources will come from the unfiltered detector, although the combination of the three detectors will provide important information regarding the time variability as a function of energy. The time resolution of the Apollo 15 instrument is 8 sec, the minimum integration time. This time permits periodicities down to approximately 5 sec and random variability of approximately 10 sec to be detected.

Deployment and Operation of the Instrument

The instrument, hard-mounted in the SIM bay of the CSM, is used for the galactic X-ray astronomical observations during the transearth-coast phase of the mission by pointing the instrument at a cosmic X-ray source and continuously counting for a sustained period. The spacecraft is required to hold the pointing position accurately to within 1° for approximately 1 hr of observation. The integrated count output for each of the three counters is recorded successively in 8-sec periods. Signals are divided into eight channels of pulse amplitude. A summary of the observing schedule is given in table 17-III. Two of the objects, Sco X-1 and Cyg X-1, were observed simultaneously in radio waves by the Westerbork Observatory, and Sco X-1 was observed simultaneously in visible light by the Crimean Astrophysical Observatory and the Wise Observatory. The X-ray spectrom-

TABLE 17-III.--*Apollo 15 Astronomical X-Ray Schedule*

Source	*Start, GET, hr:min*	*Duration of observation, min:sec*	*Date*	*G.m.t., hr:min*
Centaurus	226:28	1:05	August 5	00:02
Midgalactic latitude	237:15	0:50	August 5	10:49
Scorpius	245:45	0:35	August 5	19:19
Cygnus	246:35	0:55	August 5	20:09
South galactic pole	261:50	0:55	August 6	11:24
North galactic pole	274:15	0:30	August 6	23:49
Galactic plane anticenter	275:00	1:00	August 7	00:34

eter can be operated either in a normal-gain mode, in which the pulse height or energy channels are concentrated on the region 0.7 to 3 keV, or in an attenuate mode, in which all energies are doubled. Except for the first pointing position, the instrument was in the normal-gain mode. The X-ray source observed in the first pointing position is known to be deficient in photons below 3 keV. Consequently, the instrument was placed in the attenuate mode for that position.

The FOV of the instrument is 30° by 30°, or approximately 1 sr of solid angle. This FOV is rather large--so large that, if the instrument were pointed directly at Sco X-1 and Cyg X-1, other neighboring sources would be in the FOV at the same time. To avoid these potentially confusing difficulties, pointing positions were intentionally chosen to be several degrees off the source. As a result, the full intensity of the sources was not observed.

The origin of a rather strong component of diffuse cosmic X-rays is still unknown. The flux contained 1 sr that is actually greater than that of almost all the discrete sources. One of the outstanding questions of X-ray astronomy is whether this flux is truly isotropic or whether there is increased emission from relatively nearby clusters of galaxies. If the flux is isotropic to a high degree, the flux originates from sources at very large distances, possibly at the edge of the universe. The diffuse flux should not show any time variability. Several of the pointing positions, numbers 2, 5, 6, and 7, did not include discrete sources, only diffuse X-ray background. There were two reasons for devoting some of the time to observing the diffuse flux: (1) to determine the degree of isotropy and (2) to provide a control of the ability to determine time variability. If variability is observed in these positions, there is an indication of extraneous systematic effects in the instrument, in the data transmission, or in the method of analysis.

Results

Preliminary results from the observations of Sco X-1 and Cyg X-1 have been obtained from analysis of the quick-look or thrift data. There are indications of variability in the count rate; however, the apparent intensity of a source is a function of the angle from which the source is viewed. A change of 1° in the angle will cause an apparent intensity change of 1.5 percent. Consequently, spurious variations in the intensity of a source are induced by spacecraft motion. Because records of the spacecraft attitude during the pointing positions were not available for this section, no definite conclusions can be made concerning the relationship of observed variability effects to the source.

The count rate as a function of time for Sco X-1 is shown in figure 17-15. Data are not included for several time intervals because of the appearance of calibration sources. In the final data analysis, the contribution of the calibration sources will be subtracted, and the missing intervals will be supplied. The X-ray data are shown for two intervals of energy, 1 to 3 keV and >3 keV. The former is the sum of all the events in channels 1 to 7, and the latter is the interval of energy for channel 8. Two features are seen qualitatively in the data. A weak quasi-cyclical variation in intensity exists for three periods of approximately 5-min duration, and a very pronounced increase in the X-ray counting rate occurred at the end of the Apollo observations. Both features appear in both energy intervals. These effects are statistically significant, and if the effects are not caused by

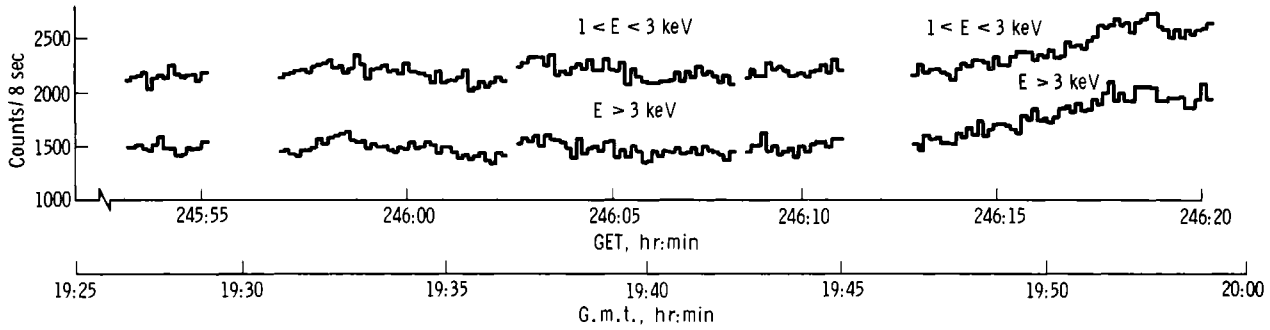

FIGURE 17-15.–The X-ray counting rate of Sco X-1 in two energy (E) bands as a function of time as observed during the Apollo 15 mission. Data have been omitted during periods when a calibration source appears.

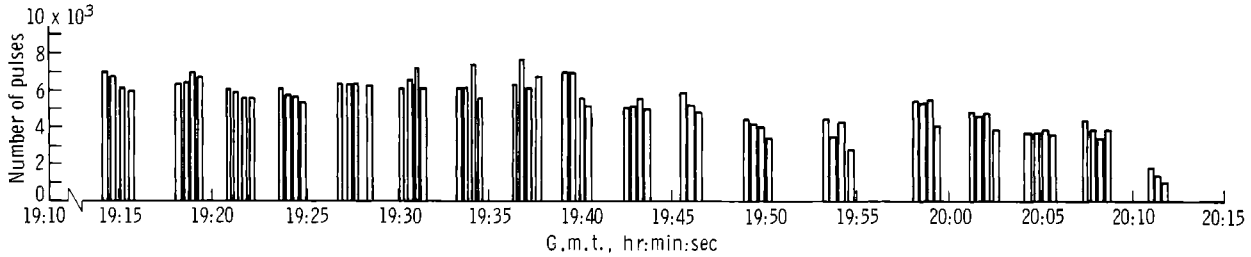

FIGURE 17-16.–Optical flux of Sco X-1 at the time of the Apollo 15 X-ray observation.

changes in spacecraft attitude, the statistics indicate that Sco X-1 is varying rapidly.

Data from simultaneous optical observations by the Crimean Astrophysical Observatory are shown in figure 17-16. Sky background has been subtracted. The statistical precision of these data is approximately 1 to 2 percent smaller than the apparent variations in optical density; however, systematic effects that could lead to variations have not been investigated. Discounting possible corrections for systematic errors, the X-ray intensity increases simultaneously as the optical intensity decreases. Several minutes of data from Cyg X-1 observation are shown in figure 17-17. The large peak is the appearance of a calibration source. The 8-sec time resolution of the instrument is insufficient to reveal the very rapid time variations that are described in reference 17-16. However, a statistically significant rise and fall in intensity begins at approximately 246 hr 57 min GET and ends at approximately 247 hr 03 min GET. In this case also, the possible factor of spacecraft motion is still in question.

Summary

The Apollo 15 X-ray detector was sucessfully pointed at three pulsating X-ray sources and at four locations dominated by the diffuse X-ray flux. During the observation period, the count rate from Sco X-1 and Cyg X-1 showed statistically significant changes of approximately 10 percent in intensity during a period of several minutes; however, possible changes in spacecraft attitude might account for the variations. Simultaneous optical observations of Sco X-1 by the Crimean Astrophysical Observatory tentatively indicate an anticorrelation between changes in X-ray and optical intensities during the final minutes of the Apollo observations. If the increase in flux of Sco X-1 observed during the Apollo 15 mission is not a result of changes in spacecraft attitude, the change in the X-ray intensity of Sco X-1 will be the most rapid ever observed.

Final analysis of the Apollo data will necessarily involve a comparison with UHURU results that cover different time regimes. The fast time resolution of the

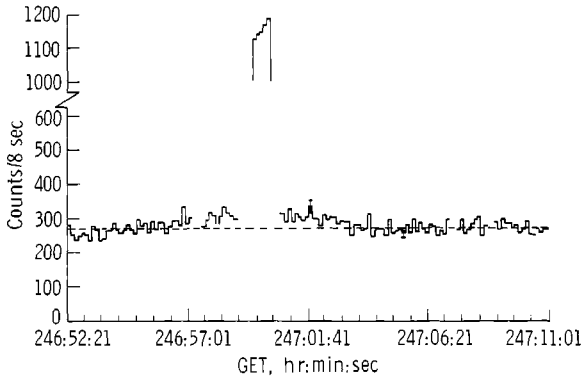

FIGURE 17-17.–The X-ray flux of Cyg X-1 during 13 min of 1-hr observation during the Apollo 15 mission. A dashed horizontal line representing a constant intensity is shown for reference. The large peak is the effect of a calibration source.

spacecraft is only 8 sec, whereas the superior time of the UHURU is 0.1 sec. Because UHURU is an orbiting satellite, short-duration observations can be made during several days, but the ability in the Apollo missions to monitor variations continuously for approximately 1 hr will fill an important gap in the observation of the pulsating sources.

REFERENCES

17-1. Adler, I.; Gorenstein, P.; Gursky, H.; and Trombka, J.: Advances in X-Ray Analysis. vol. 13. Plenum Press, 1970.

17-2. Adler, Isidore: X-Ray Emission Spectrography in Geology. Elsevier (New York), 1966.

17-3. Pohn, H. A.; and Wildey, R. L.: A Photoelectric-Photographic Study of the Normal Albedo of the Moon. Part A, Lunar and Planetary Investigation. Astrogeologic Studies, Dec. 1966, pp. 211-234.

17-4. Soderblom, L. A.: The Distribution and Relative Ages of Regional Lithologies in the Lunar Maria. Abstracts with Programs, vol. 2, no. 70, Geol. Soc. Am. 1970 Annual Meeting, pp. 690-691.

17-5. Carr, M. H.: Geologic Map of the Mare Serenitatis Region of the Moon. U.S. Geological Survey, Misc. Geol. Inv. Map I, p. 489.

17-6. Wilhelms, D. E.: Summary of Telescopic Lunar Stratigraphy. Part A, Lunar and Planetary Investigation. Astrogeologic Studies Annual Progress Report, July 1, 1965, to July 1, 1966, pp. 235-298.

17-7. Marvin, U. B.; Wood, J. A.; Taylor, G. J.; Reid, J. B.; et al.: Relative Proportions and Probable Sources of Rock Fragments in the Apollo 12 Soil Samples. Proceedings of the Second Lunar Science Conference, vol. 1, A. A. Levinson, ed., MIT Press (Cambridge, Mass.), 1971, pp. 679-700.

17-8. Levinson, A.A., ed.: Proceedings of the Apollo 11 Lunar Science Conference. Pergamon Press (New York), 1970.

17-9. Mason, Brian; and Melson, William G.: The Lunar Rocks. John Wiley & Sons, Inc., 1970.

17-10. Levinson, A. A., ed.: Proceedings of the Second Lunar Science Conference. MIT Press (Cambridge, Mass.), 1971.

17-11. Vinogradov, A. P.: Preliminary Data on Lunar Ground Brought to Earth by Automatic Probe Luna 16. Proceedings of the Second Lunar Science Conference, vol. 1, A. A. Levinson, ed., MIT Press (Cambridge, Mass.), 1971, pp. 1-16.

17-12. Lunar Sample Preliminary Examination Team: Preliminary Examination of Lunar Samples from Apollo 14. Science, vol. 173, no. 3998, Aug. 20, 1971, pp. 681-693.

17-13. McKay, D. S.; Morrison, D. A.; Clanton, U. S.; Ladle, G. H.; et al.: Apollo 12 Soil and Breccia. Proceedings of the Second Lunar Science Conference, vol. 1, A. A. Levinson, ed., MIT Press (Cambridge, Mass.), 1971, pp. 755-774.

17-14. Meyer, C.; Brett, R.; Hubbard, N. J.; Morrison, D. A.; et al.: Mineralogy, Chemistry, and Origin of the KREEP Component in Soil Samples from the Ocean of Storms. Proceedings of the Second Lunar Science Conference, vol. 1, A. A. Levinson, ed., MIT Press (Cambridge, Mass.), 1971, pp. 393-412.

17-15. Chernov, G. M.; Kirnozov, F. F.; Surkov, I. A.; and Vinogradov, A. P.: Measurements of γ Radiation of the Moon's Surface by the Cosmic Station Luna 10. Geochemistry (USSR), vol. 8, 1966, p. 891.

17-16. Oda, M.; Gorenstein, P.; Gursky, H.; Kellogg, E.; et al.: X-ray Pulsations from Cygnus X-1 Observed from UHURU. Ap. J. (Letters), vol. 166, no. 1, May 1971, p. L1.

17-17. Giacconi, R. ; Gursky, H.; Kellogg, E.; Schreier, E.; et al.: Discovery of Periodic X-ray Pulsations in Centaurus X-3 from UHURU. Ap. J. (Letters), vol. 167, no. 2, July 1971, p. L67.